Journal of Carbon Research

MDPI

Article

Adsorption of H_2 on Penta-Octa-Penta Graphene: Grand Canonical Monte Carlo Study

Maxim N. Popov [1,*], Thomas Dengg [1], Dominik Gehringer [2] and David Holec [2]

[1] Materials Center Leoben (MCL) Forschung GmbH, Roseggerstrasse 12, A-8700 Leoben, Austria [2] Department of Materials Science, Montanuniversität Leoben, Franz-Josef-Strasse 18, A-8700 Leoben, Austria

* Correspondence: maxim.popov@mcl.at

Received: 28 February 2020; Accepted: 23 March 2020; Published: 1 April 2020

Abstract: In this paper, we report the results of hydrogen adsorption properties of a new 2D carbon-based material, consisting of pentagons and octagons (Penta-Octa-Penta-graphene or POP-graphene), based on the Grand-Canonical Monte Carlo simulations. The new material exhibits a moderately higher gravimetric uptake at cryogenic temperatures (77 K), as compared to the regular graphene. We discuss the origin of the enhanced uptake of POP-graphene and offer a consistent explanation.

Keywords: Carbon-based materials; graphene; POP-graphene; Octa-Penta-grapnene; hydrogen storage; physical adsorption; adsorption isotherm; Grand-Canonical Monte Carlo (GCMC)

1. Introduction

Using hydrogen as an energy carrier instead of fossil fuels is hugely desirable due to ecological reasons, but one of the pillars of hydrogen economy—hydrogen storage—still remains a pressing issue. Numerous approaches are being developed to store hydrogen, ranging from the use of high-pressure vessels to exploiting reversibly chemically bound hydrogen [1–4]. Yet, another possibility is using adsorbent materials. Although metal-organic-frameworks (MOFs) exhibit the highest H_2 adsorption capacities, carbon-based materials are still attracting a lot of attention [3–5] because they can be a cheap and environmentally friendly alternative. When produced with the help of biotechnologies, carbon-based materials have a potential to not only achieve zero, but even negative-CO_2 emission–via binding CO_2 from the atmosphere in the process of photosynthesis. Different carbon-based structures are being considered in experiments, e.g., nanoporous spongy graphene [6], few-layer graphene flakes [7], or even nanoscaled activated carbon cloth [8], to mention a few. Also theoretically, a multitude of carbons are considered, among them carbon nanotubes [9,10], pillared graphene [11], sandwiched graphene–fullerene composite [12], or nanohorns and nanocones [13]. There are also attempts to improve the adsorption properties of carbon-based materials using dopants, e.g., metal atoms [14–16]. Recently, a new carbon-based material was reported, Penta-Octa-Penta graphene, or POP-graphene [17], sometimes also referred to as Octa–Penta–Graphene (OPG) [18]. The discovery was preceded by the work of Chen and co-workers [19], who have demonstrated a controlled creation of line defects in graphene consisting of pentagons and octagons, formed upon electron beam irradiation and Joule heating. So far, POP-graphene has only been studied in the context of Li-ion batteries as an electrode material [17,18]. It is hence the aim of this work to investigate the hydrogen adsorption properties of POP-graphene and compare its performance to that of graphene.

2. Methods

To compute the adsorption properties of the considered materials, we used the Grand–Canonical Monte Carlo (GCMC) [20] approach as implemented in the LAMMPS [21,22] code. For each considered

system, we performed 2×10^6 Monte Carlo cycles, each amounting to 100 attempts to add/remove a H_2 molecule and 100 attempts to change the position of randomly chosen H_2 molecules already present in the simulation box. By monitoring the evolution of the state variables (energy, pressure, and particle numbers) and their moving averages, it was established, that skipping the first 0.5×10^6 MC cycles is sufficient for the purpose of reliable sampling within equilibrium part of the MC trajectory. To take into account the deviations of the H_2 gas from the ideal behavior (fugacity), we always computed the pressure for the given value of the H_2 chemical potential in a separate GCMC simulation of H_2 gas in the same simulation box as for the adsorption simulation, but without the 2D carbon.

3. Structural Models

The structures of graphene and POP-graphene are depicted in Figure 1.

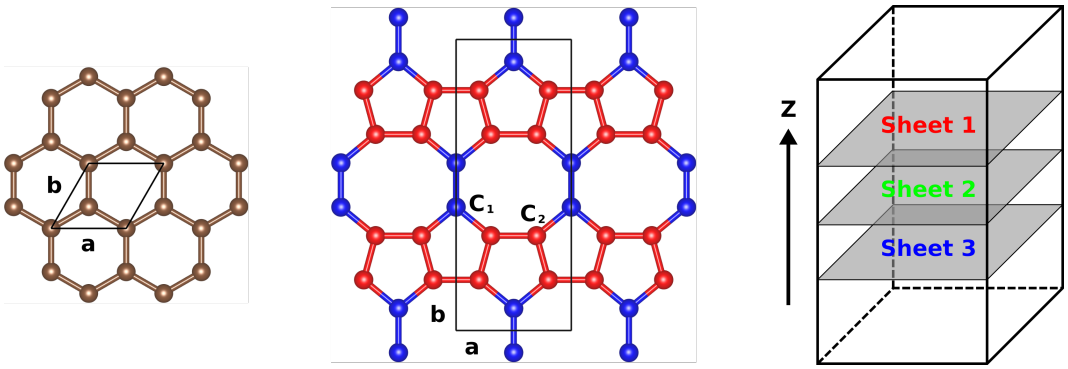

Figure 1. Structures of: (**left**) graphene and (**middle**) POP-graphene. Black lines show the borders of the unit cells. In the case of POP-graphene, the inequivalent carbon atoms (C_1 and C_2) are color-coded. (**Right**) Slit-pore geometry with 3 carbon sheets in the simulation box.

The lattice parameters a and b of graphene were set to 2.46 Å, resulting in a bondlength of 1.42 Å. POP-graphene is a bit more complicated [17]: unlike graphene, it is non-hexagonal and has two sorts of inequivalent C atoms, C_1 and C_2. The lattice parameters a and b amounted to 3.683 Å and 9.298 Å, respectively. The bondlengths measure as follows: C_1–C_1 equals to 1.41 Å, C_1–C_2 equals to 1.44 Å, and C_2–C_2 equals to 1.46 Å. Interestingly, POP-graphene exhibits a bit higher (≈8.9%) surface area per carbon atom and hence per unit mass, as compared to graphene. We shall keep this peculiar fact in mind for the further analysis. In order to investigate the hydrogen adsorption properties of the considered 2D carbons, we employed the slit-pore geometry (see Figure 1) with one to three carbon sheets inserted in the simulation box of fixed dimensions, resulting in the interlayer spacing of 30, 15, and 10 Å, respectively. We always positioned the carbon sheets normal to the Z-axis. The geometries of the simulation boxes used in this study were as follows ($X \times Y \times Z$): graphene—rectangular supercell 27.06 Å×25.565 Å×30 Å (volume: 20.753 nm^3), POP-graphene—25.783 Å×27.894 Å×30 Å (volume: 21.575 nm^3). 3D periodic boundary conditions were maintained in all calculations.

4. Results

4.1. Interaction Potentials and Potential Fitting

Adsorption of hydrogen is often studied using classical interaction potentials among which the Lennard–Jones (LJ) potential is the most popular choice:

$$\phi_{LJ}(r_{ij}) = 4\epsilon_{ij}\left[\left(\frac{\sigma_{ij}}{r_{ij}}\right)^{12} - \left(\frac{\sigma_{ij}}{r_{ij}}\right)^{6}\right], \quad (1)$$

where r_{ij} is the distance between atoms i and j, and ϵ_{ij} and σ_{ij} are potential parameters. To describe the energy of a H_2-carbon system, we need the parameters ϵ and σ specifying the H_2–H_2 and C–H_2

interactions. The former admits two different descriptions: (1) treating the H_2 molecule as a dumbbell made of 2 H atoms and considering individual H–H interactions; (2) another possibility is to make a somewhat cruder approximation and to treat the H_2 molecule as a spherical particle. We chose to describe the H_2 molecules as spherical particles due to computational efficiency. There are a number of LJ-parametrizations available for the H_2–H_2 interactions, most notably those by Silvera [23], Buch [24], Michels [25] and its derivative proposed by Darkrim and Levesque [26]. Recently, Ustinov, Tanaka, and Miyahara [27] proposed a Mie (10-6) potential for the H_2–H_2 interactions, that seems to perform very well at cryogenic temperatures:

$$\phi_{Mie}(r_{ij}) = (25/18)15^{1/2}\epsilon_{ij}\left[\left(\frac{\sigma_{ij}}{r_{ij}}\right)^{10} - \left(\frac{\sigma_{ij}}{r_{ij}}\right)^{6}\right]. \quad (2)$$

For the purpose of this study, we selected the H_2–H_2 parameters of Darkrim–Levesque (DL) (only the LJ-part) and Ustinov–Tanaka–Miyahara (UTM). DL represents one of most widely used potentials and UTM is the latest development. Both of these potentials also offer the parameters for the C–H_2 interactions. In addition, we generated the C–H_2 potentials specific for the carbon structures of interest by fitting to the *ab initio* (vdW-DFT) data from Ref. [28]. The parameters used throughout this study are summarized in Table 1, the C–H_2 interaction potentials are also shown in Figure 2.

Table 1. Potentials and their parameters used in this work.

Source	Alias	Potential	Interaction	ϵ (meV)	σ (Å)	Notes
Darkrim-Levesque [26]	DL	LJ (12-6)	H_2–H_2	3.163	2.958	Originally from [25]
		LJ (12-6)	C–C	2.430	3.400	
		LJ (12-6)	C–H_2	2.772	3.179	Lorentz-Berthelot
Ustinov et al. [27]	UTM	Mie (10-6)	H_2–H_2	2.284	3.129	Implicit FH at 77.35 K
		Mie (10-6)	C–H_2	4.317	2.800	Implicit FH at 77.35 K
This work (graphene)	G-LJ	LJ (12-6)	C–H_2	4.951	3.037	Fit to vdW-DFT data
This work (POP-graphene)	P-LJ	LJ (12-6)	C–H_2	5.055	3.031	Fit to vdW-DFT data

At low temperature (77 K), we applied the second-order Feynman–Hibbs (FH) quantum correction to the potential to deal with the quantum effects:

$$\Delta\phi^{FH}(r) = \frac{\beta\hbar^2}{24\mu}\left[\phi''_{rr}(r) + \frac{2}{r}\phi'_{r}(r)\right], \quad (3)$$

where β is the inverse temperature $1/(k_B T)$ (k_B is the Boltzmann constant), $\hbar$ is the reduced Planck's constant, and μ is the reduced mass of the particles taking part in the interaction. When employing the potentials generated in this work, we rely upon the DL parametrization for describing the H_2–H_2 interactions.

4.2. H_2 Adsorption Properties

To quantify the adsorption capacity (or uptake), a number of definitions are in use. Here, we will stick to the gravimetric capacity, defined in the following way:

$$C_W = \frac{N_{H_2} \cdot M_{H_2}}{N_{H_2} \cdot M_{H_2} + N_C \cdot M_C} \cdot 100\%, \quad (4)$$

where N_{H_2} and N_C are the average total number of H_2 molecules and the number of carbon atoms in the simulation box, whereas M_{H_2} and M_C are their molar masses. The resulting isotherms computed at 77 and 298 K are presented in Figure 3. The 298 K isotherms computed using the UTM potential

should be taken with a grain of salt, as it is used outside of its domain of applicability (it was designed for the cryogenic temperatures).

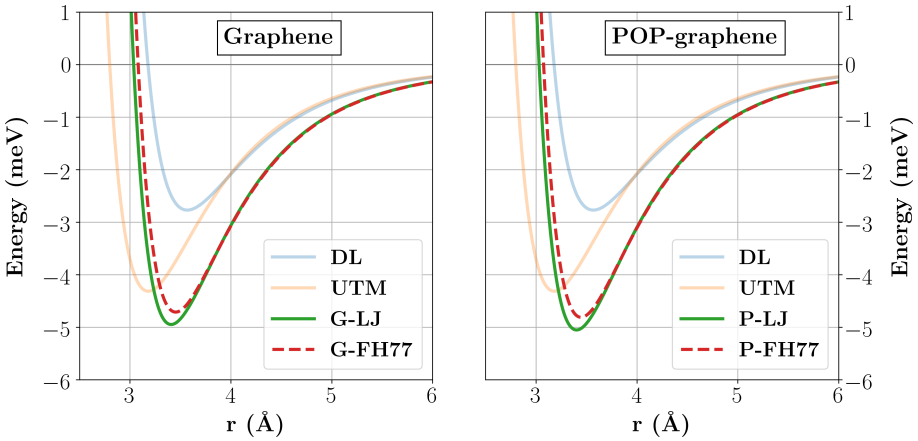

Figure 2. Comparison of the C–H_2 interaction potentials: (**left**) rraphene, (**right**) POP-graphene. The abbreviations are consistent with Table 1. The FH77 potentials are LJ potentials with the second-order Feynman–Hibbs quantum correction computed at 77 K.

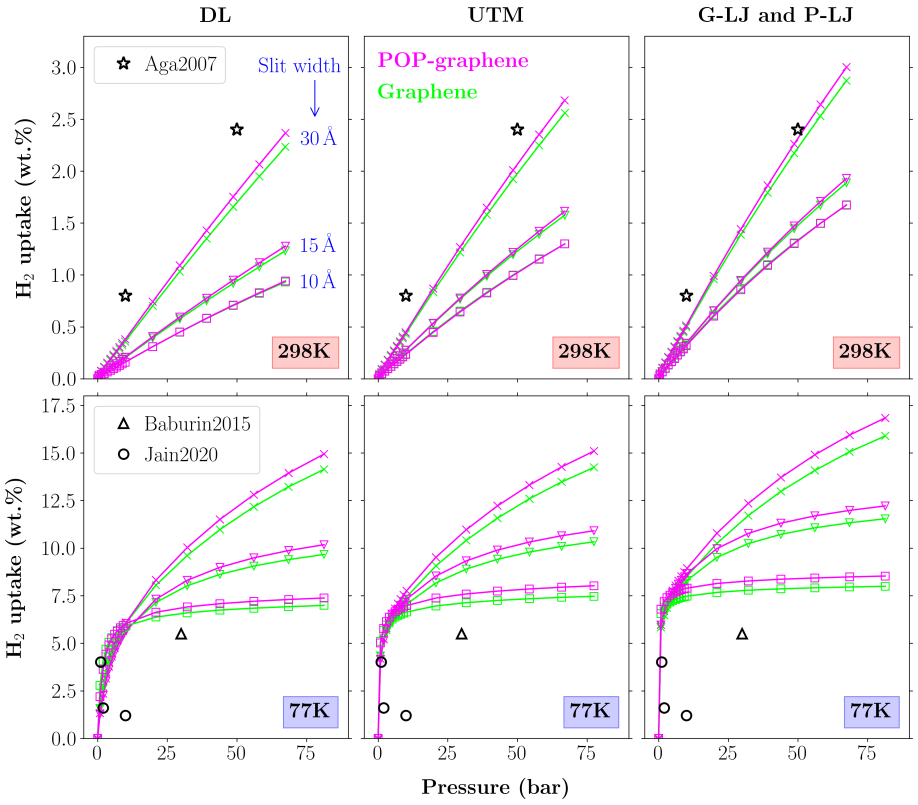

Figure 3. Gravimetric capacity/uptake (C_W) computed according to Equation (4). The references are as follows: Aga 2007 [29], Baburin 2015 [30], Jain 2020 [31].

Several observations regarding the gravimetric uptake can be made. First of all, all potentials provide a consistent picture: the gravimetric uptake of POP-graphene is moderately superior to the graphene one. Second, the slit pore width has a strong effect on the gravimetric uptake, consistent with the literature [32,33]. Third, the isotherms are in a reasonable agreement to the experimental data on pristine and modified (activated, perforated, etc.) graphene [30,31] and theoretical data on graphene [29]. Fourth, the most uptake is predicted by the potentials generated in this work and the least by the DL potential, consistent with the relative interaction strength (see Figure 1). It should also

be noticed, that different shapes of the isotherms computed at 77 K and 298 K can be well understood by considering the adsorption model of Langmuir. In particular, the nearly linear behavior at 298 K is typical of the adsorption far from completion of the first monolayer. At 77 K, we can observe formation of the full monolayer and beyond, as we shall see in Section 4.3.

Another measure of the adsorption potency is the excess gravimetric capacity, that we define as:

$$C_{EW} = \frac{\left(N_{H_2} - V_f \cdot \rho_0\right) \cdot M_{H_2}}{N_C \cdot M_C} \cdot 100\%, \tag{5}$$

where V_f is the free volume and ρ_0 is the H_2 gas density at given temperature and pressure. Here, we assume the thickness of a carbon sheet equal to 2σ, where σ is the parameter of the employed C-H_2 interaction potential (see Table 1). Hence, $V_f = (Z - 2\sigma \cdot N_S) \cdot X \cdot Y$, where N_S is the number of carbon sheets in the simulation box with dimensions $X \times Y \times Z$. The excess isotherms are presented in Figure 4.

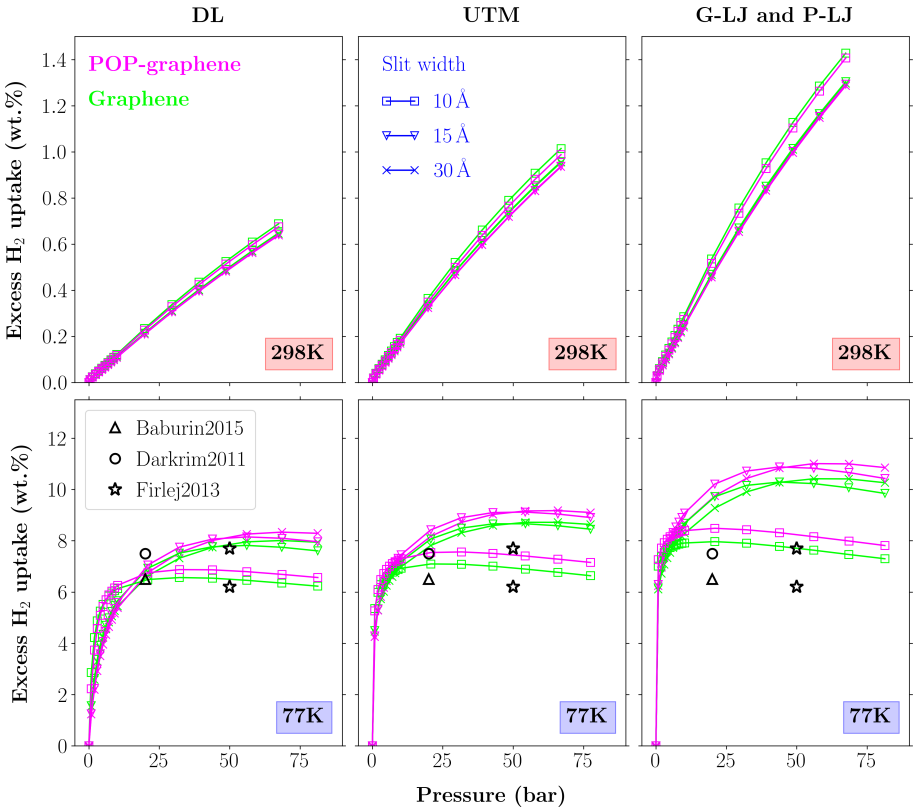

Figure 4. Excess gravimetric capacity/uptake (C_{EW}) computed according to Equation (5). The references are as follows: Baburin 2015 [30], Darkrim 2011 [32], Firlej 2013 [34].

As expected, the absolute numbers are lower as compared with the gravimetric uptake. The trends are, however, the same as at 77 K, i.e., POP-graphene being moderately superior to graphene. At 298 K, both considered carbon modifications exhibit virtually the same performance figures within the precision of our predictions, with graphene appearing marginally better. Again, the comparison to the theoretical data from literature [30,32,34] is favorable. When the effect of the slit width is considered, the following observations can be made: (1) at 77 K and pressures below ~15 bar, increasing width leads to a lower uptake; (2) at 77 K and pressures above ~25 bar, increasing width leads to a higher uptake; (3) at 298 K, narrower slits exhibit a slightly higher uptake. This behavior stems from the different densities of adsorbed hydrogen at low and elevated temperatures, and a balance between attractive and repulsive interactions in the system. At 77 K and high-pressures, the first monolayer is completely filled and adding more H_2 molecules within the same volume costs a lot of energy

due to repulsive interactions with the already-adsorbed molecules. The only way to adsorb more hydrogen is to add more layers and this needs more space. Hence, there is an increase for larger slit width. At 298 K, the densities of adsorbed hydrogen are much smaller. Even the first monolayer is not complete, because the attractive interaction of gas with the adsorbent is not strong enough for the conditions. Hence, the volume near the 2D carbon could accommodate more hydrogen molecules, if one could make the interactions with the adsorbent stronger. This is exactly what happens when the slit width is decreased, so that H_2 molecules are attracted not only by the given carbon sheet but also by its neighbor. Consequently, the smaller slit width leads to a higher uptake. The same is true for the case of 77 K and low pressures.

The last adsorption parameter, that we are going to consider, is the isosteric heat of adsorption. It is often used to characterize the average strength of the interactions between the adsorbate and the adsorbent [35]. In GCMC calculations, it can be evaluated using the formula:

$$Q_{st} = k_B T - \frac{\langle NE \rangle - \langle N \rangle \langle E \rangle}{\langle N^2 \rangle - \langle N \rangle^2}, \tag{6}$$

where N is the number of H_2 molecules and E is the energy, the $\langle\rangle$ brackets symbolize the averaging. Figure 5 shows the calculated values of Q_{st} as a function of pressure at 77 and 298 K.

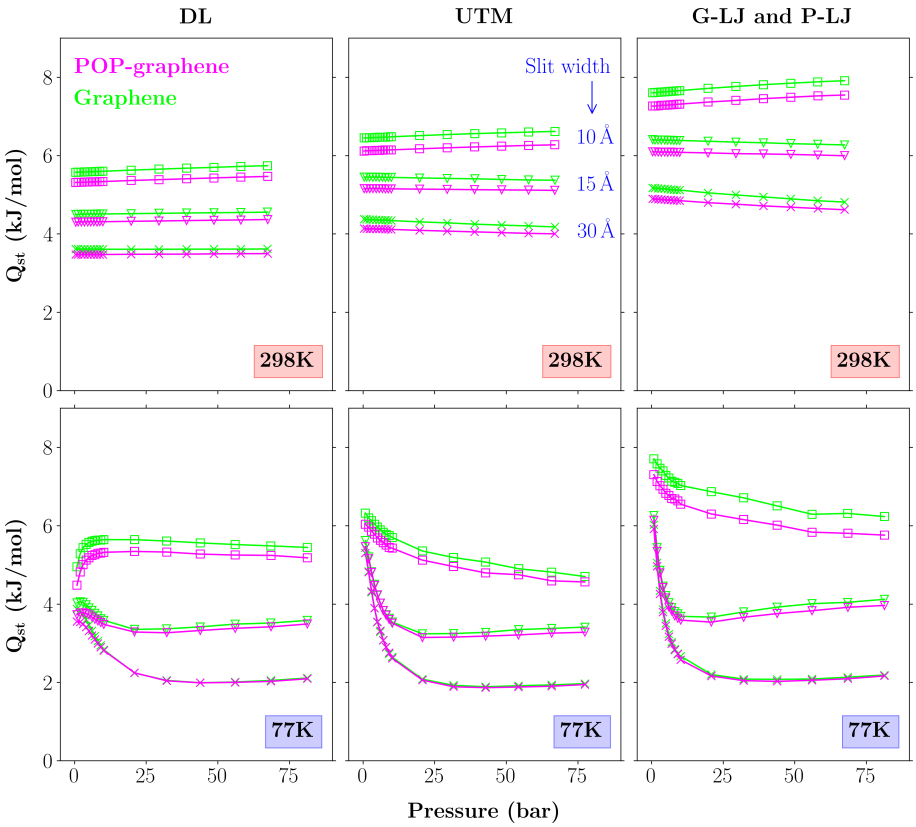

Figure 5. Isosteric heats of adsorption computed according to Equation (6).

All used potentials result in the same trends and the values of Q_{st} agree well with those typically reported for the H_2 adsorption on graphene (4–7 kJ/mol). Here, one can observe a contradictory feature: POP-graphene exhibits either comparable heat of adsorption as graphene, or even lower values; however, we have already seen that POP-graphene slightly outperforms graphene, when the (excess) gravimetric uptake is considered. This discrepancy could, potentially, be resolved by recalling that POP-graphene has a higher area per C atom (also, per unit mass), so, even though the binding strength is lower as compared to graphene, the higher area per C atom allows POP-graphene to pull a

bit ahead in the gravimetric uptake. This hypothesis could be verified and, to this end, we look closer into the average H_2 distributions.

4.3. Average H_2 Density Distribution

We will start with the H_2 density profiles computed along the Z-axis shown in Figure 6. Here, we consider only the data computed at 77 K using the potentials generated in this work. To see the confinement effects, we compute the profiles for all considered slit widths.

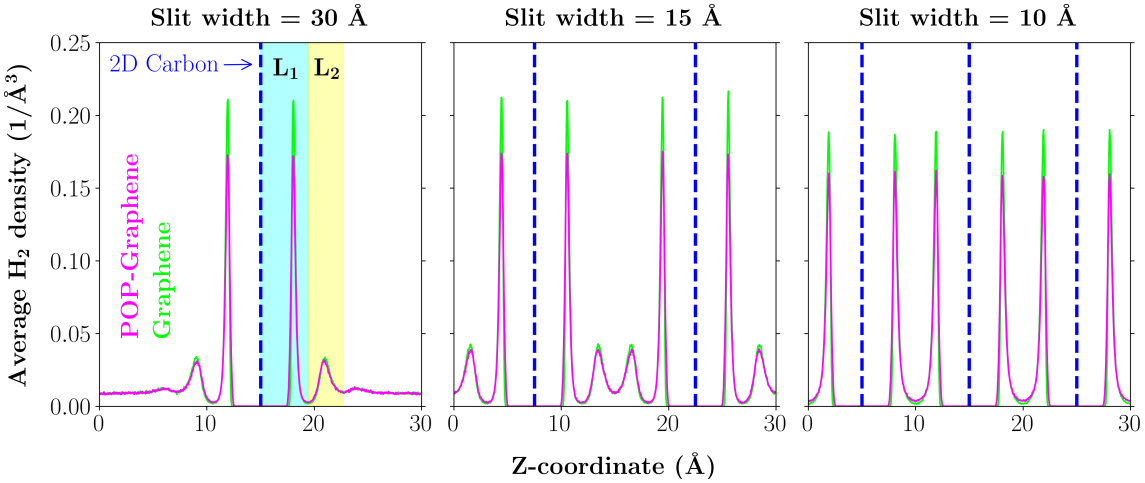

Figure 6. Average H_2 density profiles along the direction normal to the 2D carbon sheet (at 77 K and 81.3 bar) obtained using the LJ-G and LJ-P potentials. L_1 and L_2 denote the first and the second layers of adsorbed hydrogen.

Depending on the slit width, the profile exhibits 2 (for 10 Å) to 6 peaks (for 30 Å) next to a carbon sheet. They represent 1 to 3 adsorption layers on each side of the 2D carbon. It is evident, that the peak heights in the first layer of adsorbed H_2 are higher in the case of graphene, although less clear, it is also the case for the second layer. For the case of slit width of 30 Å, the area under the peaks in L_1 and L_2 is ≈3% and ≈1% bigger for graphene, respectively. In other words, the average density of adsorbed H_2 is a bit higher for graphene, as compared with POP-graphene, which is consistent with the heats of adsorption presented in Figure 5. Let us now look at the average 2D density distribution of H_2 molecules in L_1 and L_2 at the slit width of 30 Å shown in Figure 7. While the distributions in L_2 are hardly any different, there is a striking difference between distributions in L_1. In graphene, there is more or less uniform distribution of the H_2 molecules. Whereas in POP-graphene, there is a strong templating effect present. That is, graphene and POP-graphene achieve nearly the same density of adsorbed hydrogen, but in two radically different ways. It is worth noting, that the patterns seen in L_1 resemble very closely the adsorption energy maps computed for a single H_2 molecule using *ab initio* (van-der-Waals corrected DFT), presented in Reference [28]. Of course, it is a bit less of a surprise, if we recall that this DFT data was used for potential fitting. Coming back to the discrepancy observed in the Q_{st} data, it seems that our hypothesis turns out to be correct. Indeed, the average interaction strength is a bit higher for graphene as evidenced by the higher density of adsorbed hydrogen. In the case of POP-graphene the interactions are non-uniform and lead to the enhanced hydrogen adsorption in the centers of octagons, compared to graphene. However, on average, the interaction strength is slightly weaker. Given all that, ≈8.9% higher area per C atom inherent to POP-graphene appears to explain well the moderately superior gravimetric uptake.

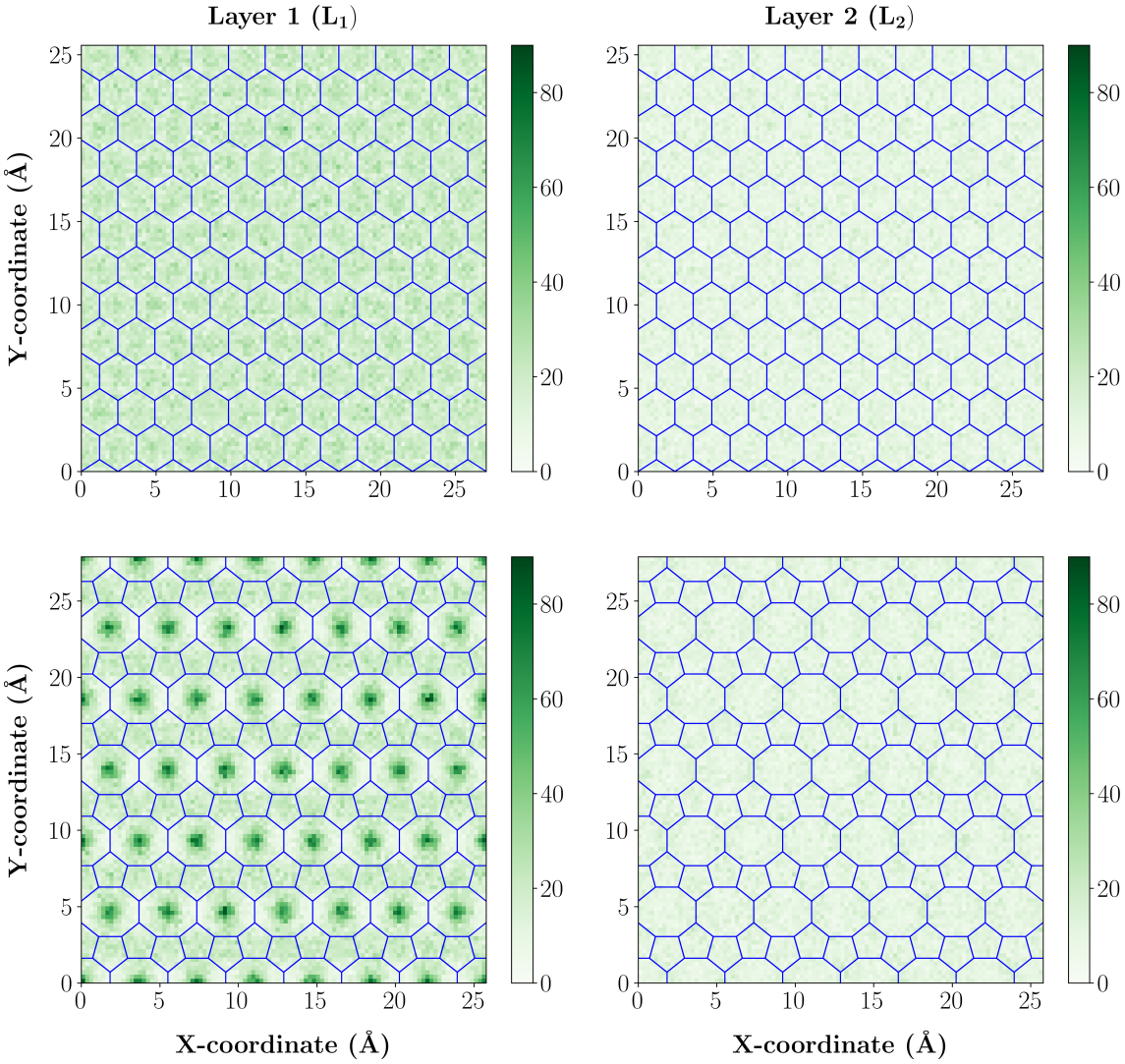

Figure 7. 2D histograms with 100 × 100 bins representing the likelihood of finding a H_2 molecule in the first two adsorption layers (see Figure 6) of: (top row) graphene and (bottom row) POP-graphene. The numbers next to the color bars denote the bin counts. Calculated from MC trajectories computed at 77 K and 81.3 bar using the LJ-G and LJ-P potentials.

5. Conclusions

In this work, we have undertaken a study of hydrogen adsorption on a new carbon-based material, Penta-Octa-Penta-graphene using a GCMC approach, based on the classical interaction potentials. To this end, we computed the adsorption isotherms and isosteric heats of adsorption at 77 and 298 K within a pressure range of 0 to ∼80 bar. We compared our data to the literature on adsorption properties of the regular graphene, and also computed regular graphene ourselves for the sake of consistent comparison. We predict that POP-graphene exhibits a moderately higher H_2 gravimetric uptake as compared to graphene at 77 K, whereas at 298 K the two carbons demonstrate nearly identical figures. Comparison of the 2D H_2 probability maps, computed for POP-graphene and graphene, revealed a striking difference in the distribution of H_2 molecules in the first adsorption layer: POP-graphene exhibits a strong templating effect, whereas graphene leads to a nearly uniform distribution. Based on the analysis of the heats of adsorption and H_2 density profiles near the carbon surface, we concluded that the superior (as compared to graphene) gravimetric uptake of POP-graphene is mostly of a geometric nature, specifically, due to higher surface area per C atom.

Author Contributions: Conceptualization, M.N.P.; methodology, M.N.P. and T.D.; validation, M.N.P., T.D., D.G., and D.H.; investigation, M.N.P. and T.D.; resources, M.N.P.; writing—original draft preparation, M.N.P.; writing—review and editing, M.N.P., T.D., D.G., and D.H.; visualization, M.N.P.; supervision, M.N.P.; funding acquisition, M.N.P. and D.H. All authors have read and agreed to the published version of the manuscript.

Funding: The authors gratefully acknowledge the financial support under the scope of the COMET program within the K2 Center "Integrated Computational Material, Process and Product Engineering (IC-MPPE)" (Project No 859480). This program is supported by the Austrian Federal Ministries for Transport, Innovation and Technology (BMVIT) and for Digital and Economic Affairs (BMDW), represented by the Austrian research funding association (FFG), and the federal states of Styria, Upper Austria and Tyrol.

Acknowledgments: The computational results presented have been achieved using the Vienna Scientific Cluster (VSC).

Conflicts of Interest: The authors declare no conflict of interest.

References

1. Kanellopoulos, N. (Ed.) *Nanoporous Materials: Advanced Techniques for Characterization, Modeling, and Processing*; CRC Press: Boca Raton, FL, USA, 2011.
2. Gadipelli, S.; Guo, Z.X. Graphene-based materials: Synthesis and gas sorption, storage and separation. *Prog. Mater. Sci.* **2015**, *69*, 1–60. [CrossRef]
3. Broom, D.; Webb, C.; Fanourgakis, G.; Froudakis, G.; Trikalitis, P.; Hirscher, M. Concepts for improving hydrogen storage in nanoporous materials. *Int. J. Hydrog. Energy* **2019**, *44*, 7768–7779. [CrossRef]
4. Hirscher, M.; Yartys, V.A.; Baricco, M.; von Colbe, J.B.; Blanchard, D.; Bowman, R.C.; Broom, D.P.; Buckley, C.E.; Chang, F.; Chen, P.; et al. Materials for hydrogen-based energy storage—Past, recent progress and future outlook. *J. Alloy. Compd.* **2019**, 827, 153548. [CrossRef]
5. Steriotis, T.; Charalambopoulou, G.; Stubos, A. Advanced Materials for Hydrogen Storage. In *Nanoporous Materials: Advanced Techniques for Characterization, Modeling, and Processing*; Kanellopoulos, N., Ed.; CRC Press: Boca Raton, FL, USA, 2011; pp. 513–547.
6. Kostoglou, N.; Constantinides, G.; Charalambopoulou, G.; Steriotis, T.; Polychronopoulou, K.; Li, Y.; Liao, K.; Ryzhkov, V.; Mitterer, C.; Rebholz, C. Nanoporous spongy graphene: Potential applications for hydrogen adsorption and selective gas separation. *Thin Solid Film.* **2015**, *596*, 242–249. [CrossRef]
7. Kostoglou, N.; Tarat, A.; Walters, I.; Ryzhkov, V.; Tampaxis, C.; Charalambopoulou, G.; Steriotis, T.; Mitterer, C.; Rebholz, C. Few-layer graphene-like flakes derived by plasma treatment: A potential material for hydrogen adsorption and storage. *Microporous Mesoporous Mater.* **2016**, *225*, 482–487. [CrossRef]
8. Kostoglou, N.; Koczwara, C.; Prehal, C.; Terziyska, V.; Babic, B.; Matovic, B.; Constantinides, G.; Tampaxis, C.; Charalambopoulou, G.; Steriotis, T.; et al. Nanoporous activated carbon cloth as a versatile material for hydrogen adsorption, selective gas separation and electrochemical energy storage. *Nano Energy* **2017**, *40*, 49–64. [CrossRef]
9. Kuzubov, A.A.; Popov, M.N.; Fedorov, A.S.; Kozhevnikova, T.A. A theoretical study of the dissociative chemisorption of hydrogen on carbon nanotubes. *Russ. J. Phys. Chem. A Focus Chem.* **2008**, *82*, 2117–2121. [CrossRef]
10. Kuzubov, A.A.; Avramov, R.P.; Raimova, M.A.; Popov, M.N.; Milyutina, Y.M.; Kozhevnikova, T.A.; Artyushenko, P.V. Modeling and calculations of the physicochemical parameters of diffusion of atomic hydrogen on the surface of differently sized nanotubes with different chiralities. *Russ. J. Phys. Chem. A* **2009**, *83*, 649–653. [CrossRef]
11. Dimitrakakis, G.K.; Tylianakis, E.; Froudakis, G.E. Pillared Graphene: A New 3-D Network Nanostructure for Enhanced Hydrogen Storage. *Nano Lett.* **2008**, *8*, 3166–3170. [CrossRef]
12. Ozturk, Z.; Baykasoglu, C.; Kirca, M. Sandwiched graphene-fullerene composite: A novel 3-D nanostructured material for hydrogen storage. *Int. J. Hydrog. Energy* **2016**, *41*, 6403–6411. [CrossRef]
13. Gotzias, A.; Heiberg-Andersen, H.; Kainourgiakis, M.; Steriotis, T. A grand canonical Monte Carlo study of hydrogen adsorption in carbon nanohorns and nanocones at 77K. *Carbon* **2011**, *49*, 2715–2724. [CrossRef]
14. Kuzubov, A.A.; Krasnov, P.O.; Kozhevnikov, T.A.; Popov, M.N. Calculation of the energy of binding of titanium and scandium complexes to the surface of carbon nanotubes. *Russ. J. Phys. Chem. B* **2009**, *3*, 679–683. [CrossRef]

15. Kuzubov, A.A.; Krasnov, P.O.; Kozhevnikova, T.A.; Popov, M.N.; Artyushenko, P.V. Peculiarities of the decoration of carbon nanotubes with transition metal atoms. *Russ. J. Phys. Chem. B* **2011**, *5*, 163–167. [CrossRef]
16. Holec, D.; Kostoglou, N.; Tampaxis, C.; Babic, B.; Mitterer, C.; Rebholz, C. Theory-guided metal-decoration of nanoporous carbon for hydrogen storage applications. *Surf. Coatings Technol.* **2018**, *351*, 42–49. [CrossRef]
17. Wang, S.; Yang, B.; Chen, H.; Ruckenstein, E. Popgraphene: A new 2D planar carbon allotrope composed of 5–8–5 carbon rings for high-performance lithium-ion battery anodes from bottom-up programming. *J. Mater. Chem. A* **2018**, *6*, 6815–6821. [CrossRef]
18. Gao, P.; Zhang, Y.; Chen, X.; Wu, Z.; Zhang, Q.; Zhang, S. OPGs: Promising anode materials with high specific capacity and rate capability for Li/Na ion batteries. *Nanoscale* **2018**, *10*, 17942–17948. [CrossRef]
19. Chen, J.H.; Autès, G.; Alem, N.; Gargiulo, F.; Gautam, A.; Linck, M.; Kisielowski, C.; Yazyev, O.V.; Louie, S.G.; Zettl, A. Controlled growth of a line defect in graphene and implications for gate-tunable valley filtering. *Phys. Rev. B* **2014**, *89*, 121407. [CrossRef]
20. Frenkel, D.; Smit, B. *Understanding Molecular Simulation: From Algorithms to Applications*, 2nd ed.; Computational Science Series; Academic Press: Cambridge, MA, USA, 2002.
21. Plimpton, S. Fast Parallel Algorithms for Short-Range Molecular Dynamics. *J. Comput. Phys.* **1995**, *117*, 1–19. [CrossRef]
22. Large-Scale Atomic/Molecular Massively Parallel Simulator (LAMMPS). Available online: http://lammps.sandia.gov (accessed on 28 February 2020).
23. Silvera, I.F. The solid molecular hydrogens in the condensed phase: Fundamentals and static properties. *Rev. Mod. Phys.* **1980**, *52*, 393–452. [CrossRef]
24. Buch, V. Path integral simulations of mixed para-D2 and ortho-D2 clusters: The orientational effects. *J. Chem. Phys.* **1994**, *100*, 7610–7629. [CrossRef]
25. Michels, A.; de Graaff, W.; Seldam, C.T. Virial coefficients of hydrogen and deuterium at temperatures between −175 °C and +150 °C. Conclusions from the second virial coefficient with regards to the intermolecular potential. *Physica* **1960**, *26*, 393–408. [CrossRef]
26. Darkrim, F.; Levesque, D. Monte Carlo simulations of hydrogen adsorption in single-walled carbon nanotubes. *J. Chem. Phys.* **1998**, *109*, 4981–4984. [CrossRef]
27. Ustinov, E.; Tanaka, H.; Miyahara, M. Low-temperature hydrogen-graphite system revisited: Experimental study and Monte Carlo simulation. *J. Chem. Phys.* **2019**, *151*, 024704. [CrossRef]
28. Gehringer, D.; Dengg, T.; Popov, M.N.; Holec, D. Interactions between a H_2 Molecule and Carbon Nanostructures: A DFT Study. *C J. Carbon Res.* **2020**, *6*, 16. [CrossRef]
29. Aga, R.S.; Fu, C.L.; Krčmar, M.; Morris, J.R. Theoretical investigation of the effect of graphite interlayer spacing on hydrogen absorption. *Phys. Rev. B* **2007**, *76*, 165404. [CrossRef]
30. Baburin, I.A.; Klechikov, A.; Mercier, G.; Talyzin, A.; Seifert, G. Hydrogen adsorption by perforated graphene. *Int. J. Hydrog. Energy* **2015**, *40*, 6594–6599. [CrossRef]
31. Jain, V.; Kandasubramanian, B. Functionalized graphene materials for hydrogen storage. *J. Mater. Sci.* **2020**, *55*, 1865–1903. [CrossRef]
32. Lamari, F.D.; Levesque, D. Hydrogen adsorption on functionalized graphene. *Carbon* **2011**, *49*, 5196–5200. [CrossRef]
33. Dicko, M.; Seydou, M.; Lamari, F.D.; Langlois, P.; Maurel, F.; Levesque, D. Hydrogen adsorption on graphane: An estimate using ab-initio interaction. *Int. J. Hydrog. Energy* **2017**, *42*, 10057–10063. [CrossRef]
34. Firlej, L.; Kuchta, B.; Lazarewicz, A.; Pfeifer, P. Increased H_2 gravimetric storage capacity in truncated carbon slit pores modeled by Grand Canonical Monte Carlo. *Carbon* **2013**, *53*, 208–215. [CrossRef]
35. Builes, S.; Sandler, S.I.; Xiong, R. Isosteric Heats of Gas and Liquid Adsorption. *Langmuir* **2013**, *29*, 10416–10422. [CrossRef] [PubMed]